Supporting Information

A sulfur-containing fluorescent hybrid porous polymer for selective detection and adsorption of Hg^{2+} ions

Zhuo Lv, *Zixu Chen, Shengyu Feng, Dengxu Wang,* Hongzhi Liu*

National Engineering Research Center for Colloidal Materials & Key Laboratory of Special Functional Aggregated Materials, Ministry of Education, Shandong Key Laboratory of Advanced Organosilicon Materials and Technologies, School of Chemistry and Chemical Engineering, Shandong University, Jinan 250100, P. R. China

*Corresponding author's e-mail: dxwang@sdu.edu.cn

Table of contents

Characterization

Fig. S9 The fluorescence quenching photographs of HPP-SH suspensions (0.1 mg/mL) after adding Hg^{2+} ions (100 ppm) under UV light.

Fig. S10 The fluorescence emission spectra of the suspensions (0.1 mg/mL) of HPP-SH-2.5; HPP-SH-5 and HPP-SH (λ_{ex} = 365 nm).

Fig. S11 The LOD was obtained by the linear relationship between emission intensity of HPP-SH-2.5 suspension and the concentrations of Hg^{2+} from 0 to 10 ppm.

Fig. S12 The LOD was obtained by the linear relationship between emission intensity of HPP-SH-5 suspension and the concentrations of Hg^{2+} from 0 to 10 ppm.

Fig. S13 Equilibrium adsorption isotherm evaluated by the Freundlich model.

Fig. S14 Adsorption kinetics estimated by the pseudo-first-order model.

Fig. S15 High-resolution spectra of Hg4f after adsorption of Hg^{2+} by HPP-SH.

Fig. S16 BET plots of HPP-1 (r = 0.999952, C = 211.901).

Fig. S17 BET plots of HPP-SH-2.5 (r = 0.999918, C = 280.638)

Fig. S18 BET plots of HPP-SH-5 (r = 0.999969, C = 252.011)

Fig. S19 BET plots of HPP-SH (r = 0.999904, C = 267.780).

Table S1 The elemental analysis of HPP-SH before and after 380° heating.

Table S2 Porosity data of HPP-1 and HPP-SH.

Table S3 Porosity data of HPP-1 and HPP-SH in harsh conditions.

Table S4 The absolute quantum yields of HPP-1 and HPP-SH with and without other metal ions.

Table S5 The parameters of LOD for HPP-SH.

Table S6 The parameters of LOD for HPP-SH-2.5.

Table S7 The parameters of LOD for HPP-SH-5.

Table S8 The Langmuir isotherm model parameters for the adsorption of Hg2+ by HPP-SH.

Table S9 The Freundlich isotherm model parameters for the adsorption of Hg^{2+} by HPP-SH.

Table S10 Kinetic parameters for the adsorption of Hg^{2+} by HPP-SH.

Characterization. Fourier transform infrared (FT-IR) spectra were measured within a 4000 to 400 cm^{-1} region and recorded on a Bruker TENSOR-27 infrared spectrophotometer (KBr pellet). Solid-state ^{13}C and ^{29}Si cross-polarization/magic-angle-spinning (CP/MAS) NMR spectra were recorded on a Bruker AVANCE-500 NMR spectrometer operating at a magnetic field strength of 9.4 T. The resonance frequencies at this field strength were 125 and 99 MHz for ^{13}C and ^{29}Si NMR, respectively. A chemagnetics 5 mm triple-resonance MAS probe was used to acquire ^{13}C and ^{29}Si NMR spectra. ^{29}Si MAS NMR spectra with high power proton decoupling were recorded by using a p/2 pulse length of 5 ms, a recycle delay of 120 s, and a spinning rate of 5 kHz. Elemental analyses were conducted using an Elementar vario EL III elemental analyzer.

Thermogravimetric analysis (TGA) was performed under N_2 using a TA SDTQ600 from 30 °to 800 °C with a heating rate of 10 °C min^{-1}. Contact angles were recorded by using a Dataphysics OCA-20 contact angle analyzer with distilled water as the test liquid. Powder X-ray diffraction (PXRD) was performed by a Riguku D/MAX 2550 diffractometer with Cu-Kα radiation, 40 kV, 20 mA with the 2θ range of 10°~80° (scanning rate of 10° min^{-1}). Field-emission scanning electron microscopy (FE-SEM) experiments were carried out by using HITACHI S4800 Spectrometer. The high-resolution transmission electron microscopy (HR-TEM) experiments were performed by using a JEM 2100 electron microscope (JEOL, Japan) with an acceleration voltage of 200 kV. X-ray photoelectron spectroscopy (XPS) was analysed by using the

instrument of Thermo Scientific ESCALAB 250Xi with the Al Kα radiation anode. The concentration of Hg^{2+} ions was measured by a GBC 923B-model atomic absorption spectrophotometer (AAS) (Melbourne, Australian) or inductively coupled plasma mass spectrometry (ICP-MS) (Shelton, CT, USA). Nitrogen sorption isotherm measurements were carried out on a Micro Meritics surface area and pore size analyzer. Before measurement, samples were degassed at 100 °C for at least 12 h. A sample of around 100 mg and a UHP-grade nitrogen (99.999%) gas source were used in the nitrogen sorption measurements at 77 K and collected with a Quantachrome Quadrasorb apparatus. BET surface areas were determined over a P/P_0 range from 0.01 to 0.20. Nonlocal density functional theory (NL-DFT) and Barrett-Joyner-Halenda (BJH) pore size distributions were determined by using the carbon/slit-cylindrical pore mode of the Quadrawin software. Prior to the measurements, the samples were degassed at 120 °C for at least 12 h. The fluorescent spectra of the samples were recorded with a Hitachi F-7000 fluorescence spectrophotometer using a monochromated Xe lamp as an excitation source. The absolute fluorescence quantum yields were evaluated by Rayleigh scattering using an integrating sphere and estimated using Wrighton-Ginley-Morse's method.

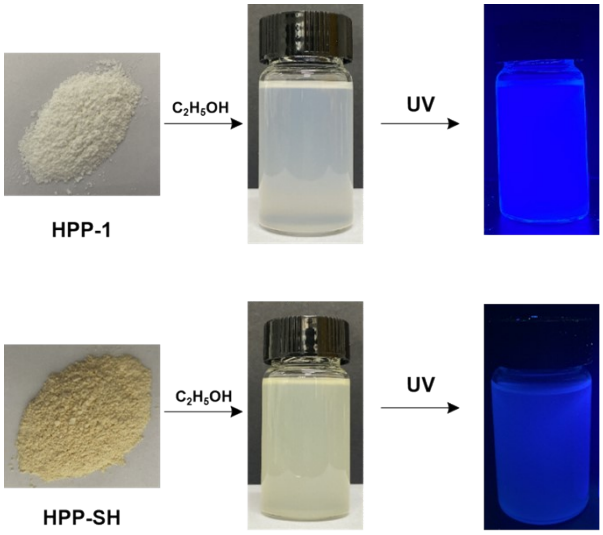

Fig. S1 The photographs of HPP-1 and HPP-SH in the solid state, and their suspensions in ethanol (0.1 mg mL^{-1}) with and without UV light

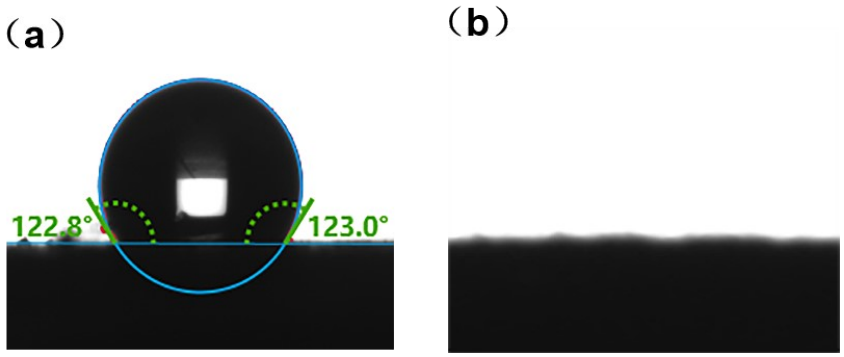

Fig. S2 Contact angle measurements of water droplets on the surface of HPP-1 (a) and HPP-SH (b)

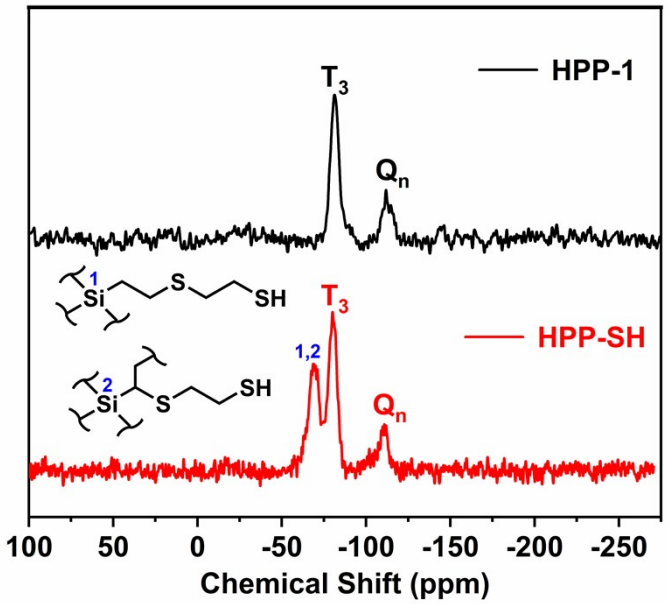

Fig. S3 ^{29}Si NMR spectra of HPP-1 and HPP-SH in the solid state.

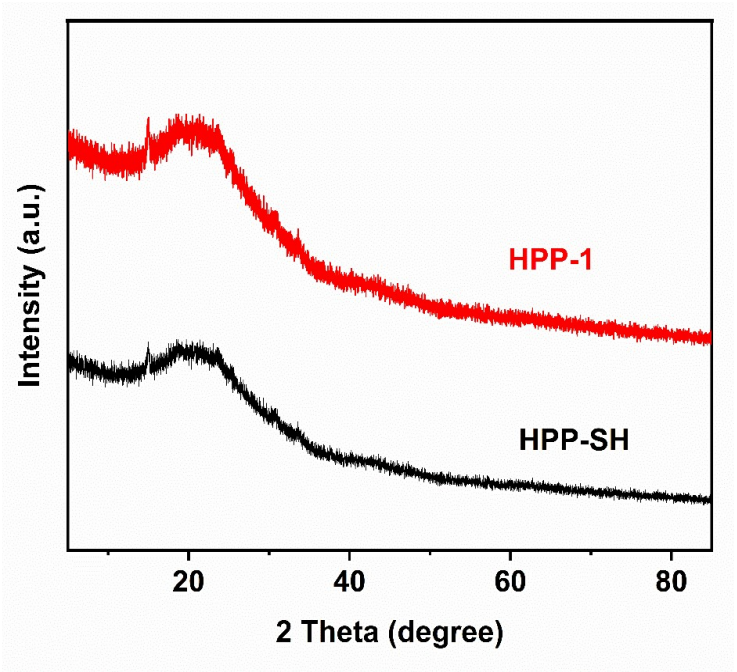

Fig. S4 XRD spectra of HPP-1 and HPP-SH

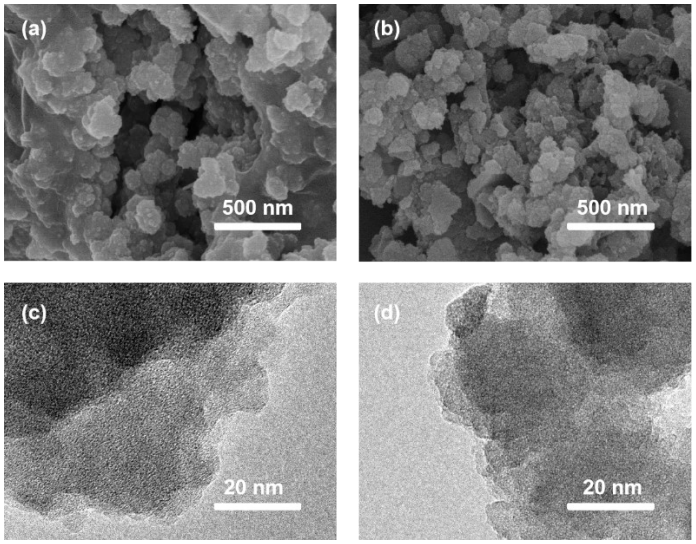

Fig. S5 SEM images of HPP-1 (a) and HPP-SH (b) and TEM images of HPP-1 (c) and HPP-SH (d)

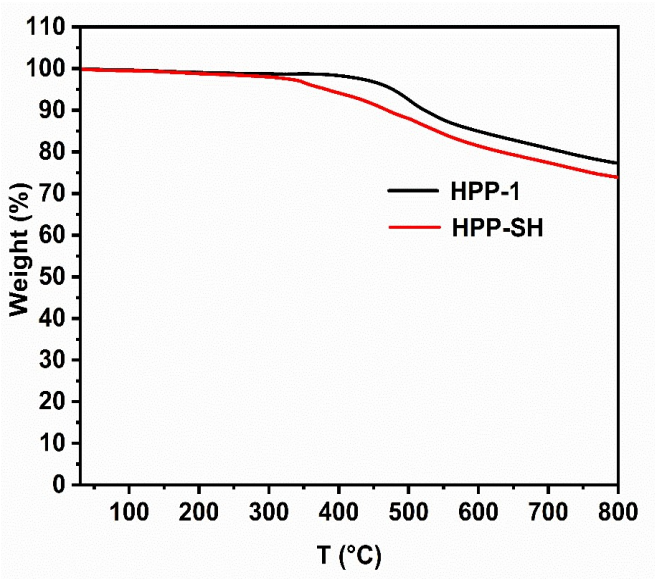

Fig. S6 TGA curves of HPP-1 and HPP-SH under N_2 atmosphere with a heating rate of 10°C min^{-1}

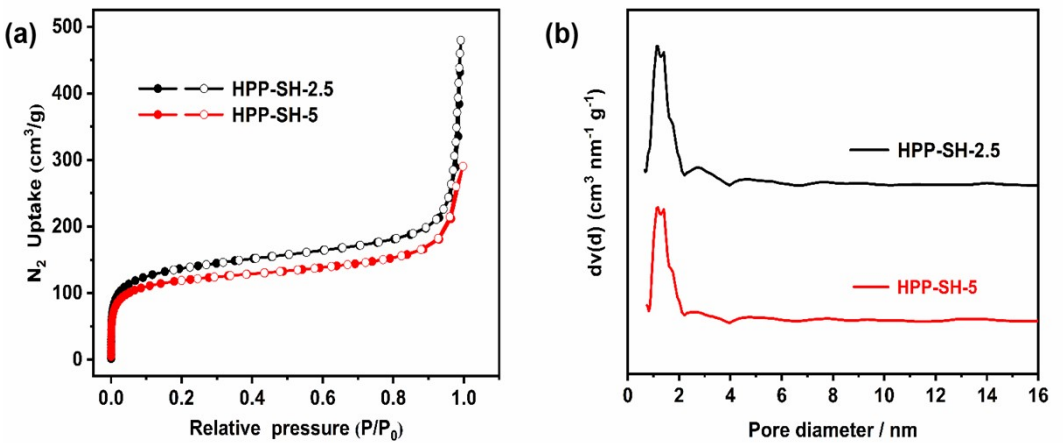

Fig. S7 (a) Nitrogen adsorption and desorption isotherms and (b) pore size distribution of HPP-SH-2.5 and HPP-SH-5 calculation based upon NLDFT

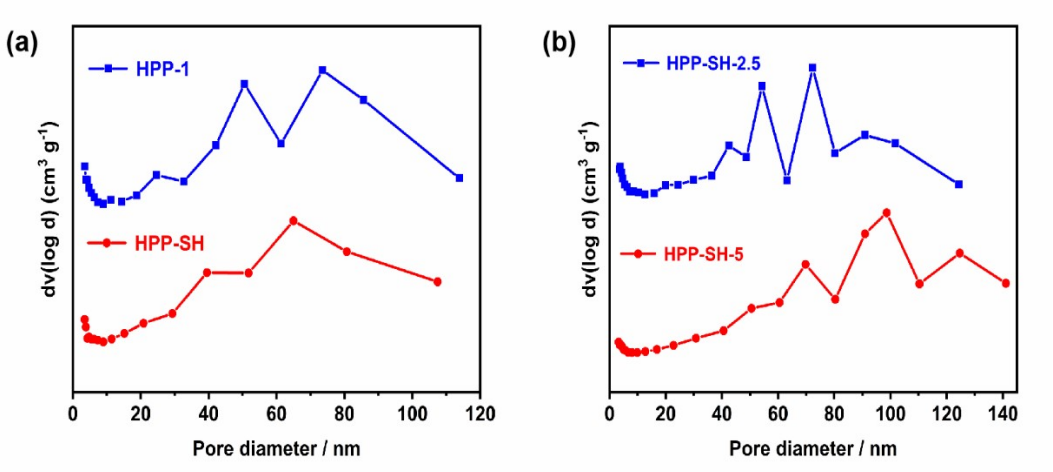

Fig. S8 The pore size distribution of HPP-1 and HPP-SH (a) and HPP-SH-2.5 and HPP-SH-5 (b) calculation based upon the BJH method

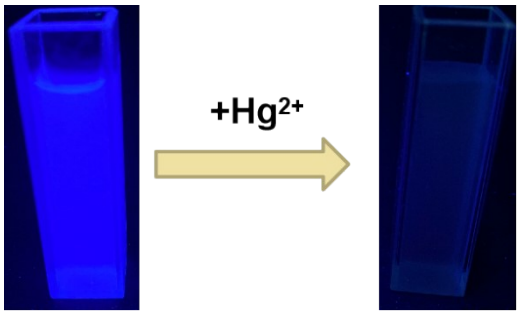

Fig. S9 The fluorescence quenching photographs of HPP-SH suspensions (0.1 mg/mL) after adding Hg^{2+} ions (100 ppm) under UV light

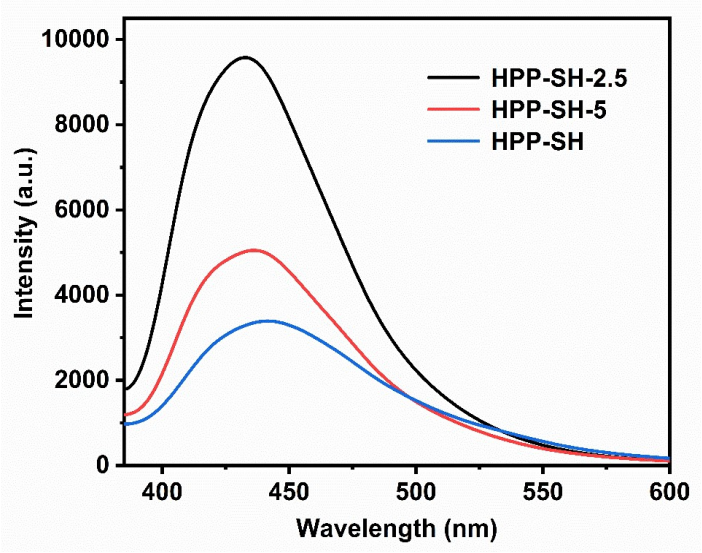

Fig. S10 The fluorescence emission spectra of the suspensions (0.1 mg/mL) of HPP-SH-2.5; HPP-SH-5 and HPP-SH (λ_{ex} = 365 nm).

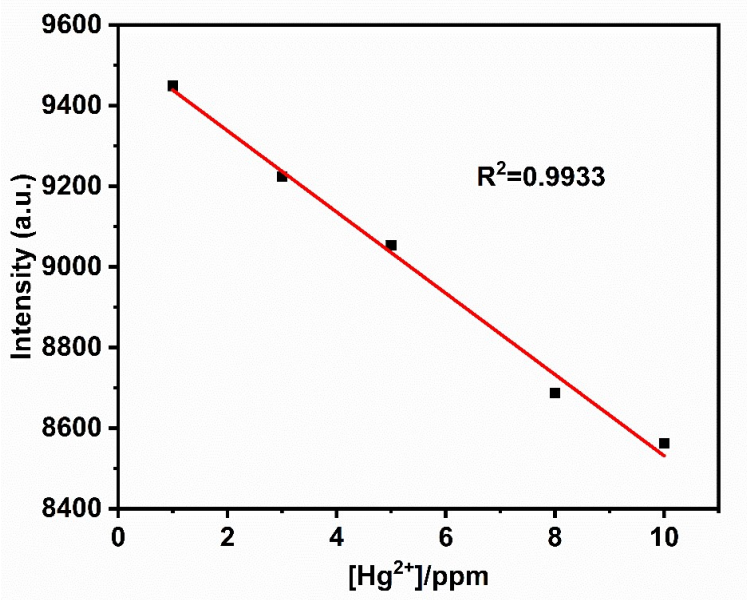

Fig. S11 The LOD was obtained by the linear relationship between emission intensity of HPP-SH-2.5 suspension and the concentrations of Hg^{2+} from 0 to 10 ppm.

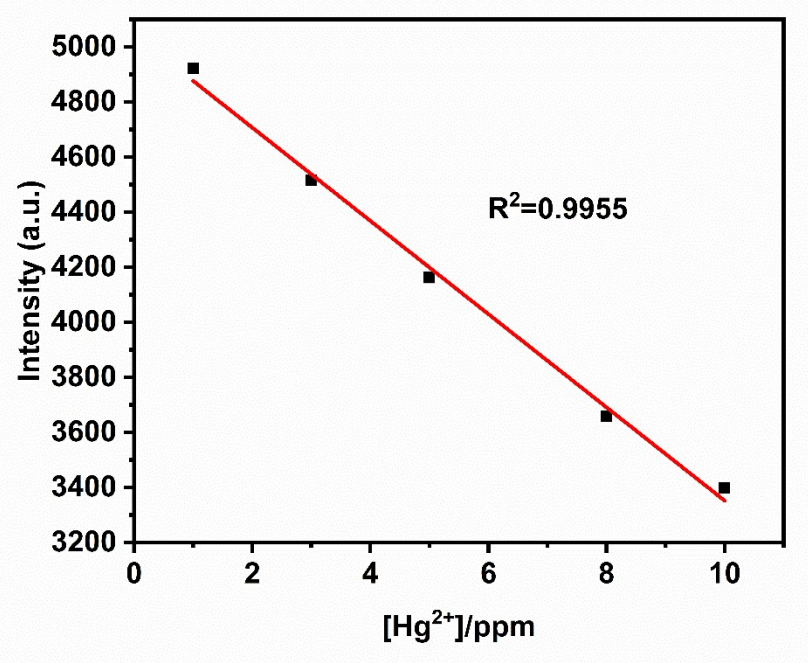

Fig. S12 The LOD was obtained by the linear relationship between emission intensity of HPP-SH-5 suspension and the concentrations of Hg^{2+} from 0 to 10 ppm.

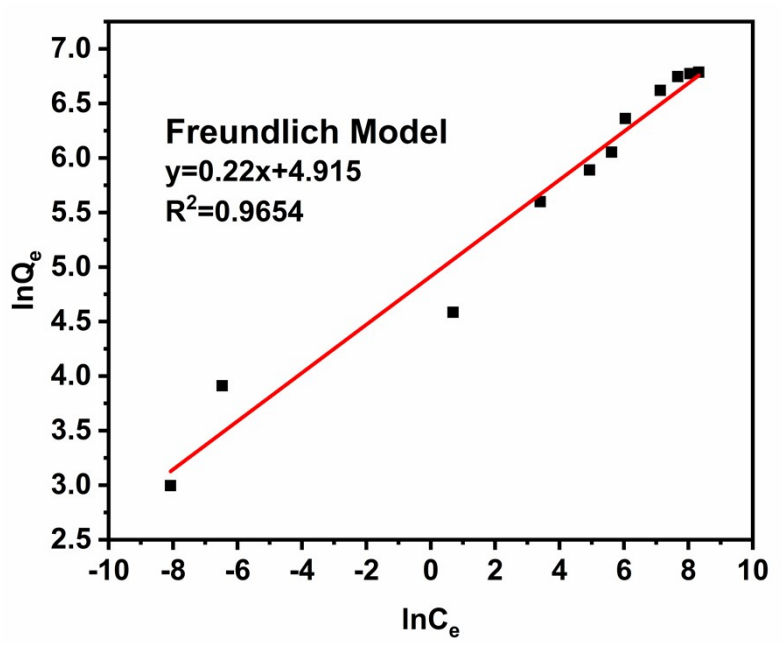

Fig. S13 Equilibrium adsorption isotherm evaluated by the Freundlich model.

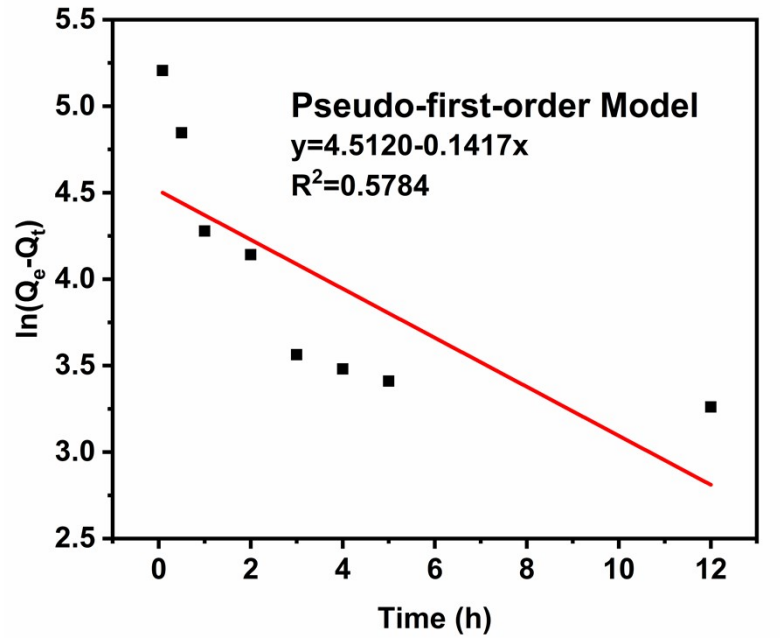

Fig. S14 Adsorption kinetics estimated by the pseudo-first-order model

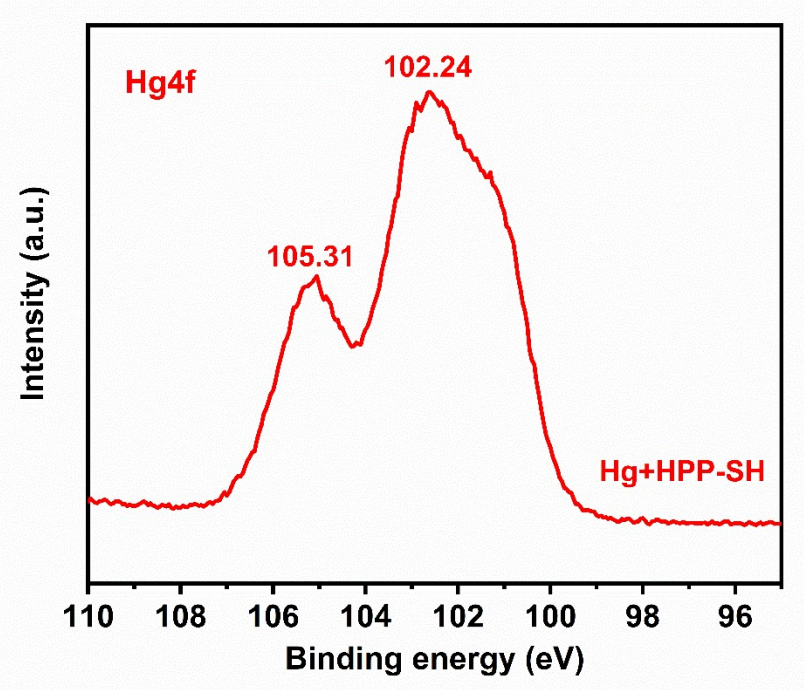

Fig. S15 High-resolution spectra of Hg4f after adsorption of Hg^{2+} by HPP-SH

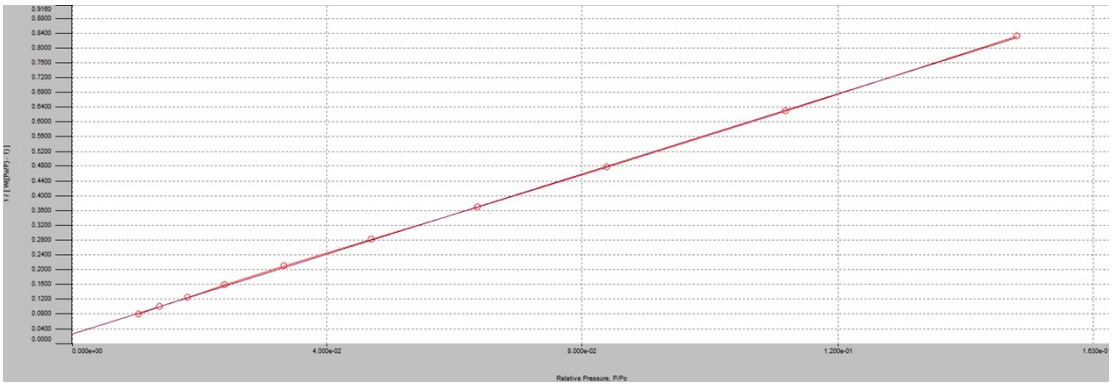

Fig. S16 BET plots of HPP-1 (r = 0.999952, C = 211.901)

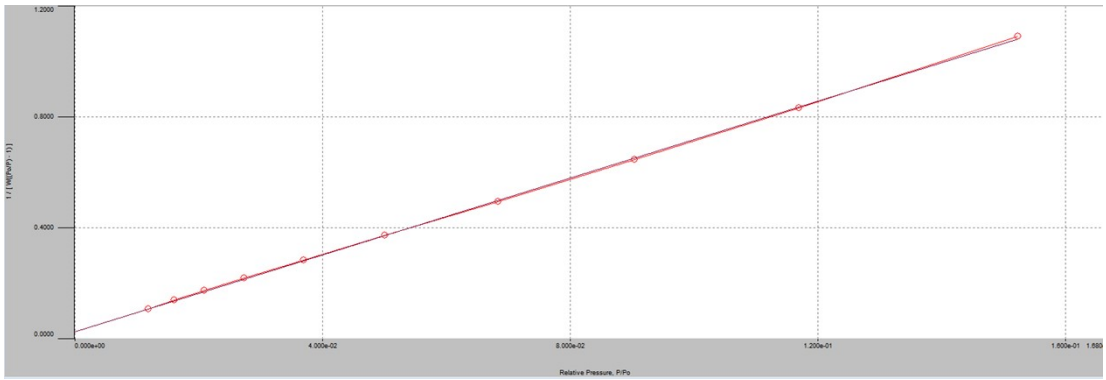

Fig. S17 BET plots of HPP-SH-2.5 (r = 0.999918, C = 280.638)

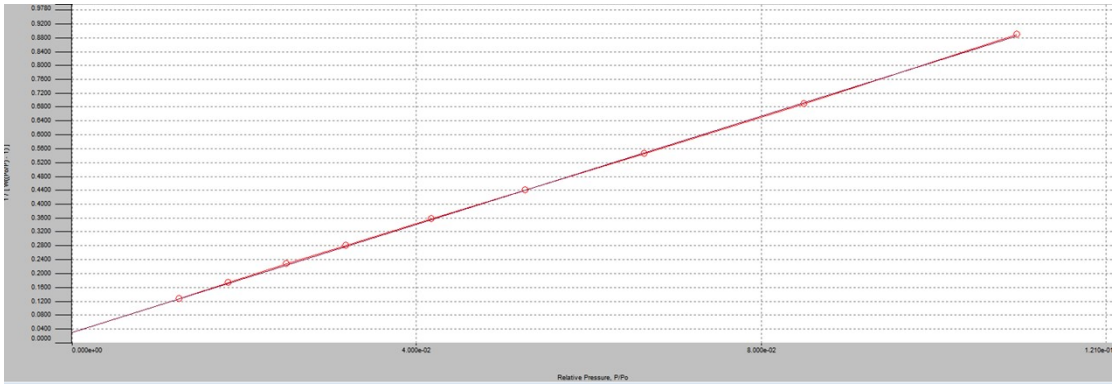

Fig. S18 BET plots of HPP-SH-5 (r = 0.999969, C = 252.011)

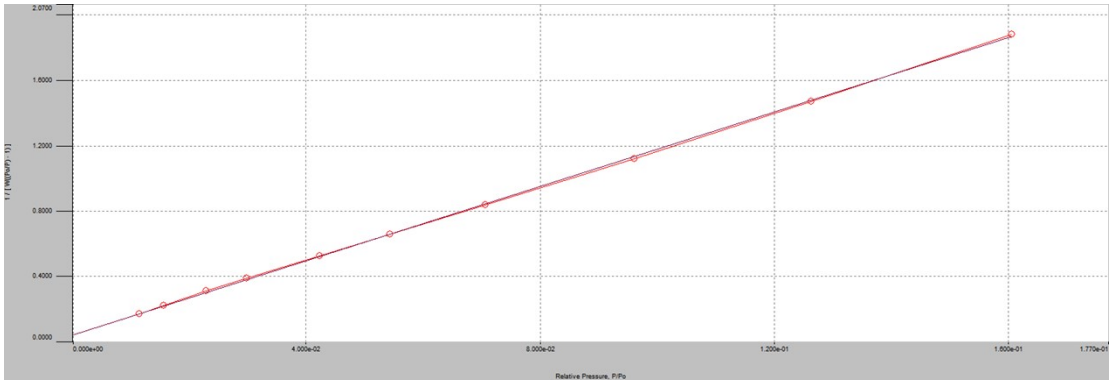

Fig. S19 BET plots of HPP-SH (r = 0.999904, C = 267.780)

Table S1 The elemental analysis of HPP-SH before and after 380° heating.

Polymers	C (wt%)	H (wt%)	S (wt%)
HPP-SH	37.07	3.81	14.44
HPP-SH after 380° heating	32.96	2.52	3.98

Table S2 Porosity data of HPP-1, HPP-SH-2.5, HPP-SH-5 and HPP-SH.

Polymers	S_{BET} (m^2g^{-1}) [a]	S_{micro} (m^2 g^{-1}) [b]	V_{total} (cm^3 g^{-1}) [c]	V_{micro} (cm^3 g^{-1}) [d]	V_{micro}/V_{total}
HPP-1	639	438	0.66	0.18	0.28
HPP-SH-2.5	501	350	0.58	0.14	0.24
HPP-SH-5	435	336	0.45	0.13	0.29
HPP-SH	305	199	0.40	0.079	0.20

[a] Surface area calculated from N_2 adsorption isotherm using the BET method; [b] Microporous surface area calculated from N_2 adsorption isotherm using t-plot method; [c] Total pore volume calculated at $P/P_0 = 0.99$; [d] Micropore volume derived using the t-plot method based on the de-Boer thickness equation.

Table S3 Porosity data of HPP-1 and HPP-SH in harsh conditions.

Polymers	pH	S_{BET} (m^2g^{-1}) [a]	S_{micro} (m^2g^{-1}) [b]	V_{total} (cm^3g^{-1}) [c]	V_{micro} (cm^3g^{-1}) [d]	V_{micro} /V_{total}
HPP-1	1	628	425	0.72	0.17	0.24
	6	621	436	0.69	0.18	0.26
	8	637	410	0.70	0.16	0.23
	13	633	443	0.71	0.19	0.27
HPP-SH	1	306	194	0.43	0.077	0.18
	6	310	203	0.40	0.082	0.21
	8	295	191	0.38	0.079	0.21
	13	320	210	0.42	0.081	0.19

[a]Surface area calculated from N_2 adsorption isotherm using the BET method; [b] Microporous surface area calculated from N_2 adsorption isotherm using t-plot method; [c] Total pore volume calculated at $P/P_0 = 0.99$; [d] Micropore volume derived using the t-plot method based on the de-Boer thickness equation.

Table S4 The absolute quantum yields of HPP-1 and HPP-SH with and without other metal ions.

	quantum yield(%)
HPP-1	15.59
HPP-1+Hg^{2+}	15.37
HPP-SH	4.41
HPP-SH+Hg^{2+}	2.10
HPP-SH+Ba^{2+}	4.32
HPP-SH+Cu^{2+}	4.18

Table S5 The parameters of LOD for HPP-SH.

	Parameters	
HPP-SH	LOD (ppb)	4.48
	σ	1.55
	K	1038.122

Table S6 The parameters of LOD for HPP-SH-2.5.

	Parameters	
HPP-SH-2.5	LOD (ppb)	50.88
	σ	1.71
	K	100.816

Table S7 The parameters of LOD for HPP-SH-5.

	Parameters	
HPP-SH-5	LOD (ppb)	27.10
	σ	1.53
	K	169.383

Table S8 The Langmuir isotherm model parameters for the adsorption of Hg^{2+} by HPP-SH

Model	Parameters	
Langmuir model	Q_m (mg/g)	900.9
	K_L (L/mg)	44.05
	R^2	0.9964

Table S9 The Freundlich isotherm model parameters for the adsorption of Hg^{2+} by HPP-SH

Model	Parameters	
Freundlich model	K_F (L/mg)	136.32
	1/n	0.22
	R^2	0.9654

Table S10 Kinetic parameters for the Hg^{2+} by HPP-SH

Model	Parameters	
Pseudo-second order	Q_e (mg/g)	370
	K_2 (h^{-1})	0.0065
	R^2	0.9988
Pseudo-first order	Q_e (mg/g)	91.1
	K_1 (g g^{-1} h^{-1})	0.1417
	R^2	0.5784